IOPscience iopscience.iop.org

Home Search Collections Journals About Contact us My IOPscience

Structural, electrical and optical properties of yttrium-doped ZnO thin films prepared by sol–gel method

This content has been downloaded from IOPscience. Please scroll down to see the full text.

2007 J. Phys. D: Appl. Phys. 40 5592

(http://iopscience.iop.org/0022-3727/40/18/014)

View the table of contents for this issue, or go to the journal homepage for more

Download details:

IP Address: 137.207.120.173
This content was downloaded on 25/09/2013 at 06:06

Please note that terms and conditions apply.

IOP Publishing Journal of Physics D: Applied Physics
J. Phys. D: Appl. Phys. **40** (2007) 5592–5597 doi:10.1088/0022-3727/40/18/014

Structural, electrical and optical properties of yttrium-doped ZnO thin films prepared by sol–gel method

Qingjiang Yu[1], Wuyou Fu[1], Cuiling Yu[1], Haibin Yang[1,3], Ronghui Wei[1], Yongming Sui[1], Shikai Liu[1], Zhanlian Liu[1], Minghui Li[1], Guorui Wang[2], Changlu Shao[2], Yichun Liu[2] and Guangtian Zou[1]

[1] National Laboratory of Superhard Materials, Jilin University, Changchun 130012, People's Republic of China
[2] Center for Advanced Optoelectronic Functional Material Research, Northeast Normal University, Changchun 130024, People's Republic of China

E-mail: yanghb@jlu.edu.cn

Received 7 June 2007, in final form 15 July 2007
Published 30 August 2007
Online at stacks.iop.org/JPhysD/40/5592

Abstract
Yttrium-doped ZnO thin films were deposited on silica glass substrates by the sol–gel method. The structural, electrical and optical properties of yttrium-doped ZnO thin films were investigated systematically and in detail. All the thin films have a preferred (0 0 2) orientation. When compared with the electrical resistivity values of films without annealing treatment, the values of films annealed in the reducing atmosphere were decreased by about three orders of magnitude. The lowest electrical resistivity value was $6.75 \times 10^{-3}\ \Omega$ cm, which was obtained in the 0.5 at% yttrium-doped ZnO thin film annealed in nitrogen with 5% hydrogen at 500 °C. In room-temperature photoluminescence (PL) spectra, two PL emission peaks are found in the pure ZnO thin film; one is the near-band-edge (NBE) emission at 3.22 eV and the other is a green emission at about 2.38 eV. Nevertheless, the green emission is not found in the PL of the yttrium-doped ZnO thin films. The low-temperature PL spectrum of the undoped ZnO thin film at 83 K is split into well-resolved free and bound excition emission peaks in the ultraviolet region, but the NBE emission of the 5 at% yttrium-doped ZnO thin film at 83 K has only one broad emission peak.

1. Introduction

ZnO is a II–VI compound semiconductor with a wide direct band gap of 3.37 eV and a large exciton binding energy of 60 meV at room temperature, which makes it a promising candidate for highly efficient, ultraviolet-light-emitting diodes and ultraviolet lasers [1–3]. Due to its piezoelectric properties, ZnO is being explored for fabricating various pressure transducers and acoustic wave and optoacoustic devices [4–6]. ZnO is also one of the promising materials for applications in transparent conductors [7], thin-film transistors [8], varistors [9], catalysts [10], gas sensors [11] and solar cells [12]. Until now high quality ZnO thin films have been fabricated by molecular beam epitaxy [13], sputtering [14], pulsed laser deposition [15], chemical vapour deposition [16], spray pyrolysis [17], sol–gel process [18–22], etc. Among them, the sol–gel technique is becoming more popular due to its simplicity, safety and low cost. Moreover, in the technique, incorporation of dopants is easy and large area substrates can be coated readily.

It is well known that the possibility of practical application of any semiconductor lies on the effective manipulation of its physical properties. Doping with selective elements offers an effective method to adjust the physical properties of semiconductors. Recently, ZnO thin films have been

[3] Author to whom any correspondence should be addressed.

successfully prepared by doping with a group III impurity, such as Al, Ga or In, using the sol–gel process [19–21]. In particular, a number of works have been carried out on aluminium-doped ZnO thin films by the sol–gel method. Ohyama *et al* [19] in their work reported the preparation of aluminium-doped ZnO thin films with highly preferential crystal orientation by the sol–gel dip-coating method. They systematically investigated the effects of aluminium doping concentration and preparation conditions on the electrical resistivity of the gel-derived films. They reported the lowest resistivity of $6.5 \times 10^{-3}\ \Omega$ cm for the 0.5 at% aluminium-doped film. However, as far as we know, yttrium-doped ZnO thin films prepared by the sol–gel process have rarely been reported. Recently, sol–gel derived yttrium-doped ZnO films have been reported by Kaur and co-workers [23, 24], but the *c*-axis preferential growth of the films was not obvious. In our latest work, transparent and conductive high preferential *c*-axis oriented ZnO thin films doped with yttrium have been prepared by the sol–gel method [25]. Herein, we are to investigate in detail the effects of yttrium doping on the structural, electrical and photoluminescence (PL) properties of ZnO thin films.

2. Experiment

The details of the preparation method of ZnO thin films have already been described in our previous work [25]. In brief, zinc acetate dehydrate ($Zn(CH_3COO)_2 \cdot 2H_2O$) and yttrium chloride ($YCl_3$) were first dissolved in a mixture of 2-methoxyethanol and MEA solution at room temperature. The molar ratio of MEA to zinc acetate was maintained at 1.0 and the concentration of zinc acetate was 0.5 M. The resultant solution was stirred at 60 °C for 2 h to yield a clear and homogeneous solution, which served as the precursor solution after cooling to room temperature.

The dip-coating method was used to coat the silica glass substrates. The drawing rate was about 6.0 cm min^{-1}. After being deposited by dip coating, the films were dried at 300 °C for 10 min to evaporate the solvent and remove organic residuals, and the process was repeated ten times. The films were then inserted into a furnace and fired in air at 550 °C for 2 h (the first post-heat treatment), followed by annealing in nitrogen with 5% hydrogen at 500 °C for 1 h (the second post-heat treatment).

The crystalline phase and crystallite orientation were determined by Rigaku D/MAX-2500 x-ray diffraction (XRD) with Cu Kα radiation. The surface and cross-section of the films were observed with a field-emission scanning electron microscope (FE-SEM) (JEOL JSM-6700F) operating at 5 KV. The electrical resistivity (ρ) and the Hall coefficient (R_H) were measured at room temperature by the van der Pauw method. The carrier concentration (N) and the Hall mobility (μ) were calculated from the electrical resistivity and the Hall coefficient using the following relations [26]:

$$N = 1/eR_H, \tag{1}$$

$$\mu = 1/Ne\rho. \tag{2}$$

The PL emission spectra were recorded with HR-800 LabRam Infinity Spectrophotometer excited by a continuous He–Cd laser with a wavelength of 325 nm. Temperature-dependent PL studies were carried out by using liquid nitrogen refrigeration equipment in the temperature range from 83 K to room temperature.

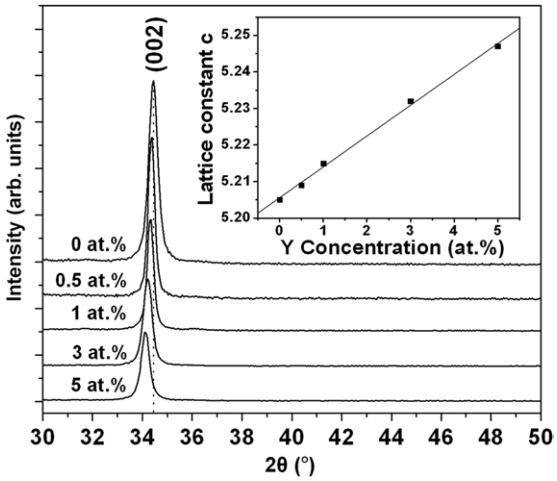

Figure 1. XRD patterns of the pure and yttrium-doped ZnO thin films with the first post-heat treatment. The inset shows the values of the lattice constant *c* of the samples at different doping concentrations. The unit of the lattice constant *c* is Angstrom.

3. Results and discussions

3.1. Structural properties

Figure 1 shows XRD patterns of the pure and doped ZnO thin films prepared during the first post-heat treatment with different yttrium concentrations (0.5, 1, 3 and 5 at%) on glass substrates. All the ZnO thin films exhibit the preferred (0 0 2) orientation. This indicates that the *c*-axis of the grains becomes uniformly perpendicular to the substrate surface, suggesting that the surface energy of the (0 0 2) plane is the lowest in ZnO crystal [27]. No yttrium oxide phases were observed, which means that some Y^{3+} ions would uniformly substitute into the Zn^{2+} sites or interstitial sites in the ZnO lattice. The peak intensities of those films decreased with increasing doping concentrations, which indicates that an increase in doping concentrations deteriorates the crystallinity of films. In addition, compared with the pure ZnO thin film, increasing yttrium concentrations caused the position shift of the doped ZnO thin films' (0 0 2) peak to lower diffraction angles. Correspondingly, the *c*-axis lattice constants of the thin films increased from 5.205 to 5.247 Å with increasing yttrium concentration, as shown in the inset of figure 1. This may be due to the fact that the ionic radius Y^{3+} (0.89 Å) is larger than that of Zn^{2+} (0.74 Å). The variation of the *c*-axis lattice constant further suggests that Y^{3+} ions replace the Zn^{2+} lattice sites or interstitial sites in the films.

Figure 2 shows FE-SEM images of the surface and cross-section of yttrium-doped ZnO thin films prepared during the first post-heat treatment with different doping concentrations. It is found that the Y doping concentration has a significant influence on the surface morphology of the ZnO thin films. The pure ZnO thin film (*a*) is composed of close-packed nanoparticles, arrayed regularly on the substrate with a narrow

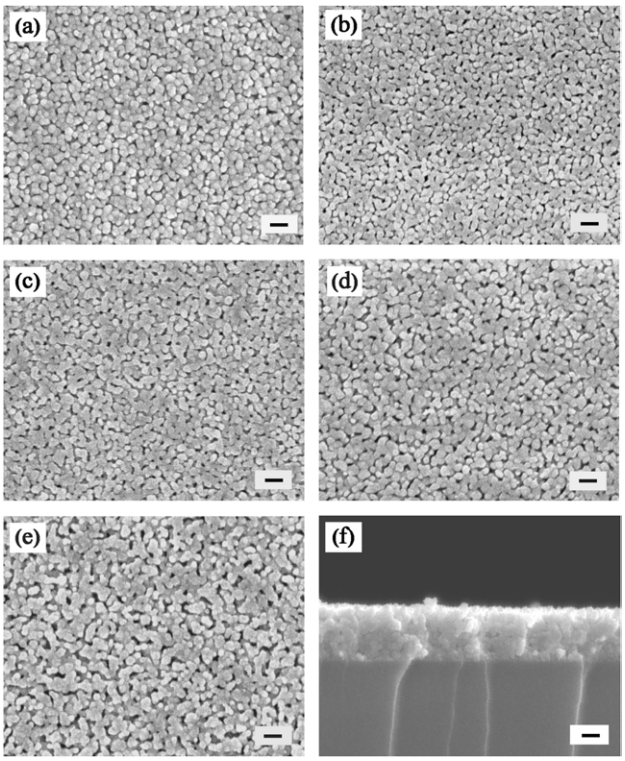

Figure 2. FE-SEM images of the surface and cross-section of yttrium-doped ZnO thin films prepared during the first post-heat treatment with different doping concentrations: (*a*) 0, (*b*) 0.5, (*c*) 1, (*d*) 3, (*e*) 5 and (*f*) 0 at%. All scale bars are 100 nm.

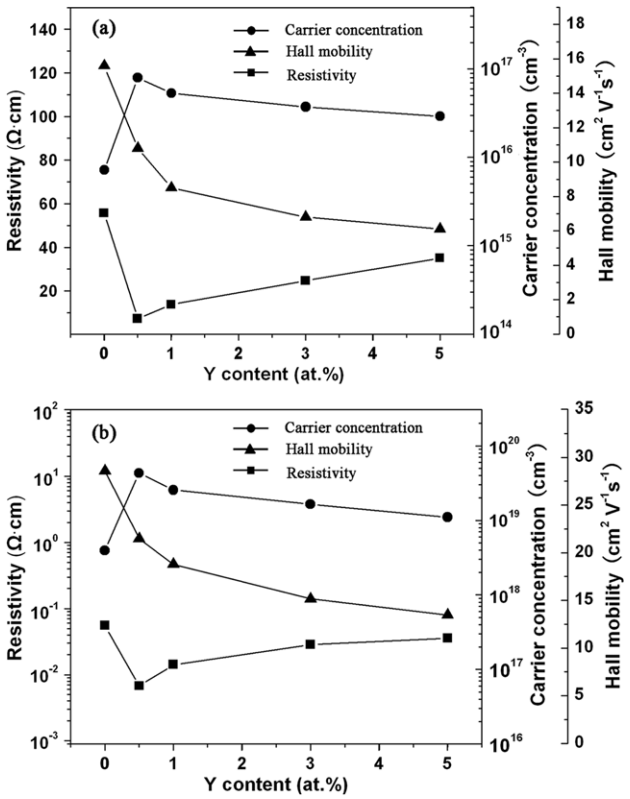

Figure 3. Variation of resistivity, carrier concentration and Hall mobility of ZnO thin films with different post-heat treatments as a function of various Y contents: (*a*) the first post-heat treatment and (*b*) the second post-heat treatment.

distribution of grain sizes. For the doped ZnO thin film (*b*)–(*e*), some agglomerated grains and a porous structure were observed; moreover, the similar morphology was more obvious with increasing yttrium doping concentration. This may be due to the formation of stresses by the difference in the ion size between zinc and yttrium. Columnar ZnO crystals, which grew together between layers and layers and formed a seriate whole, and the film's thickness of about 300 nm were observed in the cross-section image of the film (*f*).

3.2. Electrical properties

The electrical properties were investigated by Hall effect measurements. The electrical resistivity, carrier concentration and Hall mobility of ZnO thin films with different post-heat treatments as a function of various Y contents are shown in figure 3. Without regard to the second post-heat treatment, the electrical resistivity first decreased with increasing Y contents. A minimum electrical resistivity of 7.25 Ω cm was obtained at a doping content of 0.5 at%, and the corresponding carrier concentration was 7.98×10^{16} cm^{-3}, as shown in figure 3(*a*). However, by increasing the Y doping content above 0.5 at%, the electrical resistivity started to increase, and the carrier concentration started to decrease. This suggests that not all the Y atoms in the thin film contribute to donor dopants. When a small amount of Y impurities are introduced into ZnO, they mostly substitute Zn existing at lattice sites as donors, together with less Y atoms present at interstitial sites. The carrier concentration therefore increases with the Y content at first up to 0.5 at% doping. However, at higher Y contents, the carrier concentration decreases because excess Y atoms in the thin film may result in intragrain congregation and/or grain–boundary segregation forming Y–Y and Y–O clusters. These Y atoms are electrically inactive, even acting as an 'electron killer' with effects such as donor passivation; thus the electron concentrations are limited. Similar suggestions were proposed by Lu *et al* [28] and Choi *et al* [29] for ZnO : Al and ZnO : Ga films, respectively. The Hall mobility decreases gradually with the increase in the Y content in films from ∼15.6 cm^2 V^{-1} s^{-1} for pure ZnO to ∼6.1 cm^2 V^{-1} s^{-1} as the amount of Y increases to 5 at%. This may be due to the scattering from the grain boundaries and ionized impurities.

When compared with the electrical resistivity values of films without the annealing treatment, the values of films annealed in the reducing atmosphere were decreased by about three orders of magnitude. The lowest electrical resistivity value was 6.75×10^{-3} Ω cm, which was obtained in the 0.5 at% yttrium-doped ZnO thin film annealed in nitrogen with 5% hydrogen at 500 °C, as shown in figure 3(*b*). Since the electrical resistivity of ZnO is directly related to the number of electrons, electrons formed by the ionization of the interstitial zinc atoms and the oxygen vacancies affect the electrical resistivity of ZnO crystals. The decrease in resistivity of films with the second post-heat treatment was affected by both the above-mentioned cases but may be predominated by oxygen vacancies. This is because of the oxygen vacancies formed by oxygen annihilation from the ZnO crystals via the annealing process in a reducing atmosphere. In addition, when the second post-heat treatment is performed in a reducing atmosphere,

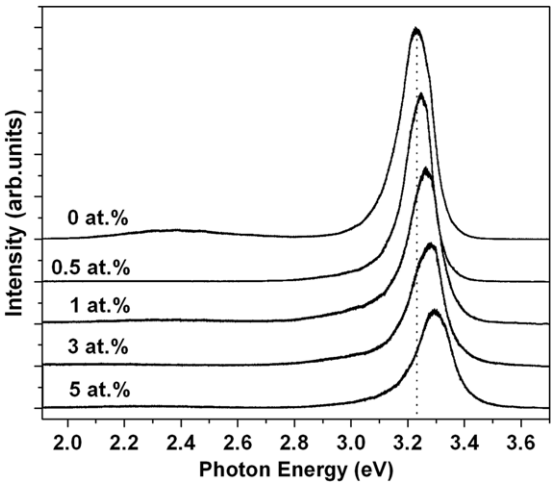

Figure 4. Room-temperature PL spectra of the pure and yttrium-doped ZnO thin films prepared during the first post-heat treatment.

the increase in the carrier concentration may be due to the desorption of oxygen in the grain boundaries which act as traps for the carriers.

3.3. Optical properties

To study the optical properties, the PL spectrum was measured using a He–Cd laser line of 325 nm as the excitation source. Figure 4 shows room-temperature PL spectra of Y doped ZnO thin films with different doping concentrations prepared during the first post-heat treatment. All ZnO thin films show a near-band-edge (NBE) emission which is attributed to a well-known recombination of free excitons (FXs), but no deep-level emissions are observed in the doped ZnO thin films. However, the PL spectrum of the pure ZnO thin film shows a very weak broad green emission at about 2.38 eV. Though the origin of the green emission is controversial, generally it is attributed to the singly ionized oxygen vacancy and the emission results from the radiative recombination of a photo-generated hole with an electron occupying the oxygen vacancy [30]. When Y was introduced into thin films, the defect PL from oxygen defects in thin films was depressed.

Compared with the pure ZnO thin film, the NBE emission peak position of the Y doped ZnO thin film has a blueshift to higher energy. As the concentration of Y increases, the NBE emission peak shifts to higher energy region. For the pure ZnO thin film, the NBE emission is located at 3.22 eV. However, the NBE emission shifts to 3.30 eV as the concentration of Y in thin film increases to 5 at%. The blueshift of NBE emission is believed to be the Burstein–Moss effect because of the doping of Y in the thin films. As we know, ZnO is naturally an n-type material, and the Fermi level will be inside the conduction band by the quantity ξ_n when it is heavily doped. Since the states below ξ_n of the conduction band are filled, the absorption edge should shift to the higher energy by ξ_n [31]. In addition, the intensity of the NBE emission peak decreases with increasing Y doping concentration, which is due to the weak exciton Coulomb interaction effect. The Y act as scattering centres of dopant and generate a screened Coulomb potential field, which makes excitons ionized because of loss of the interaction

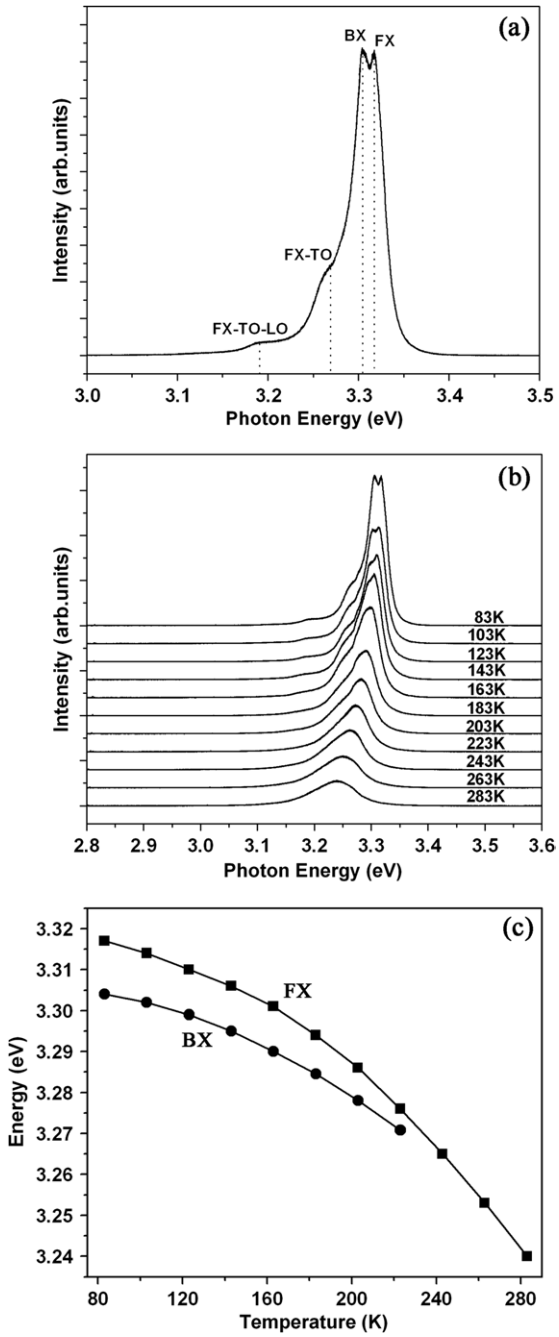

Figure 5. (*a*) PL spectrum of the pure ZnO thin film with the first post-heat treatment at 83 K. (*b*) Temperature-dependent PL spectra of the pure ZnO thin film. (*c*) Peak energies for the free- and donor-BXs as a function of temperature.

effect. As a result, the exciton effect decreases gradually with the increase in the Y doping concentration, and the intensity of the NBE emission reduces.

Figure 5(*a*) shows the PL spectrum of the pure ZnO thin film with the first post-heat treatment at 83 K. The NBE emission is split into a series of peaks. The peak at 3.317 eV is assigned to the FX recombination based on the consistency of the value with the reported result from the pure ZnO thin film [32]. The peak at 3.304 eV is attributed to the bound exciton (BX) recombination, because the difference between 3.304 and 3.317 eV is close to the activation energy of BX and

in good agreement with the reported value [32]. Two peaks located at 3.266 and 3.191 eV arise on the lower-energy side of the BX peak. The peak at 3.266 eV is attributed to the first order transverse optical (TO) phonon replica of FX recombination, because the energy spacing between this peak and the FX peak is close to the TO phonon energy (53 meV) [33]. The peak at 3.191 eV is assigned to the FX emission accompanied by TO and the first order longitudinal optical (LO) phonons (72 meV), since the energy difference between the peak and the FX is close to the sum of the energies of TO and LO phonons. It is generally accepted that the exciton–phonon coupling is governed by two mechanisms: deformation potential and Fröhlich potential. The TO scattering is mainly determined by the deformation potential related to short-range interaction. On the other hand, the LO scattering includes contributions from both the Fröhlich potential and the deformation potential [34]. In the pure ZnO thin film, the deformation potential would influence short-range interaction. Thus, there are related TO replicas.

Figure 5(*b*) shows the temperature-dependent PL spectra of the pure ZnO thin film measured from 83 to 283 K. With the increase in temperature, the intensities of all emissions are decreased and the intensity of the BX emission decreases more rapidly than that of the FX emission. The decrease in intensity is due to the thermal ionization of the BXs. In contrast, the FX emission gets relatively stronger and dominates the emission spectra when the temperature is above 243 K. The FX phonon replicas have a temperature dependence different from that of excitons, as they show a slower intensity decrease by the increase in temperature. Gradually they get weaker and broadened at higher temperatures and finally merge into the low-energy tail of the FX peak. In addition, the exciton emission of FX and BX show an obvious redshift with increasing temperature. The temperature dependence of the peak energies of FX and BX is shown in figure 5(*c*). The temperature dependence of the exciton emission energy is related to the temperature dependence of the band energy, which fits well with the following semiempirical formula:

$$E_x(T) = E_x(0) - \alpha T^2/(T + \beta), \tag{3}$$

where $E_x(0)$ is the peak energy at absolute zero temperature and α and β are the fitting parameters. $E_x(0)$ is 3.324 eV and 3.309 eV for FX and BX emissions, respectively. In figure 5(*c*), the lines represent the calculated temperature dependences for each emission mode and it is shown that the calculated lines fit well with the experimental values.

Figure 6 shows the temperature-dependent PL spectra of the 5 at% yttrium-doped ZnO thin film with the first post-heat treatment at the temperature ranging from 83 to 283 K. Compared with the pure ZnO thin film, it is interesting that the NBE emission of the 5 at% yttrium-doped ZnO thin film at 83 K is not split into a series of peaks and only one broad emission peak. FX emissions are not observed at low temperatures, which may be due to the localization of excitons by Y impurities. The broadening of the NBE emission can also account for the high concentration of intrinsic defects. The broadened emission involves excitons bound to neutral donors. With the increase of temperature, the intensity and the shift of the peak position of the NBE emissions have similar features to that of the pure ZnO thin film.

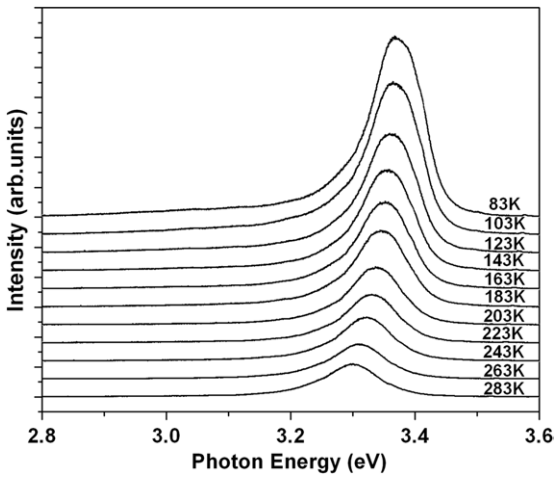

Figure 6. Temperature-dependent PL spectra of the 5 at% yttrium-doped ZnO thin film with the first post-heat treatment.

4. Conclusions

In conclusion, yttrium-doped ZnO thin films were prepared on silica glass substrates by the sol–gel method. All the thin films show preferred *c* orientation. The lattice constant *c* is found to increase with the increase in dopant concentration. When the second post-heat treatment was carried out in nitrogen with 5% hydrogen at 500 °C, the electrical resistivity value of the 0.5 at% yttrium-doped ZnO thin film dropped by about three orders of magnitude and reached $6.75 \times 10^{-3}\ \Omega$ cm. For the pure ZnO thin film, the room-temperature PL spectrum shows a strong NBE emission at 3.22 eV and a very weak deep-level emission associated with the singly ionized oxygen vacancy. Exciton emission and multiple-phonon replicas in the low-temperature PL spectrum have been identified. In particular, the first order TO photon-assisted emission of FX has been identified according to peak energy spacing. For the 5 at% yttrium-doped ZnO thin film, the shift and quenching of NBE emission, the disappearance of deep-level emission in the room-temperature PL spectrum and the absence of FX emissions in low-temperature PL spectra can be attributed to yttrium incorporation.

References

[1] Tang Z K, Wong G K L, Yu P, Kawasaki M, Ohtomo A, Koinuma H and Segawa Y 1998 *Appl. Phys. Lett.* **72** 3270
[2] Cao H, Xu J Y, Seeling E W and Chang R P H 2000 *Appl. Phys. Lett.* **76** 2997
[3] Xu H Y, Liu Y C, Liu Y X, Xu C S, Shao C L and Mu R 2005 *Appl. Phys. B: Lasers Opt.* **80** 871
[4] Yoshino Y, Makino T, Katayama Y and Hata T 2000 *Vacuum* **59** 538
[5] Gorla C R, Emanetoglu N W, Liang S, Mayo W E, Lu Y, Wraback M and Shen H 1999 *J. Appl. Phys.* **85** 2595
[6] Lee J B, Kim H J, Kim S G, Hwang C S, Hong S H, Shin Y H and Lee N H 2003 *Thin Solid Films* **435** 179
[7] Xu H Y, Liu Y C, Mu R, Shao C L, Lu Y M, Shen D Z and Fan X W 2005 *Appl. Phys. Lett.* **86** 123107
[8] Carcia P F, McLean R S, Reilly M H and Nunes G 2003 *Appl. Phys. Lett.* **82** 1117
[9] Mahan G D 1983 *J. Appl. Phys.* **54** 7
[10] Yoshimoto M, Takagi S, Umemura Y, Hada M and Nakatsuji H 1998 *J. Catal.* **173** 53

[11] Lehman H W and Widmer R 1973 *J. Appl. Phys.* **44** 3868
[12] Keis K, Magnusson E, Lindstrom H, Lindquist S E and Hagfeldt A 2002 *Sol. Energy Mater. Sol. Cells* **73** 51
[13] Look D C, Reynolds D C, Litton C W, Jones R L, Eason D B and Cantwell G 2002 *Appl. Phys. Lett.* **81** 1830
[14] Jeong S H, Kim B S and Lee B T 2003 *Appl. Phys. Lett.* **82** 2625
[15] Shan F K, Liu G X, Lee W J, Lee G H, Kim I S and Shin B C 2005 *Appl. Phys. Lett.* **86** 221910
[16] Haga K, Suzuki T, Kashiwaba Y, Watanabe H, Zhang B P and Segawa Y 2003 *Thin Solid Films* **433** 131
[17] Studenikin S A, Golgeo N and Cocivera M 1998 *J. Appl. Phys.* **83** 2104
[18] Kim Y S, Tai W P and Shu S J 2005 *Thin Solid Films* **491** 153
[19] Ohyama M, Kozuka H and Yoko T 1998 *J. Am. Ceram. Soc.* **81** 1622
[20] Cheong K Y, Muti N and Ramanan S R 2002 *Thin Solid Films* **410** 142
[21] Luna-Arredondo E J, Maldonado A, Asomoza R, Acosta D R, Meléndez-Lira M A and de la L Olvera M 2005 *Thin Solid Films* **490** 132
[22] Ohyama M, Kozuka H and Yoko T 1997 *Thin Solid Films* **306** 78
[23] Kaur R, Singh A V and Mehra R M 2005 *Phys. Status Solidi* a **202** 1053
[24] Kaur R, Singh A V, Sehrawat K, Mehra N C and Mehra R M 2006 *J. Non-Cryst. Solids* **352** 2565
[25] Yu Q, Yang H, Fu W, Chang L, Xu J, Yu C, Wei R, Du K, Zhu H, Li M and Zou G 2007 *Thin Solid Films* **515** 3840
[26] Yasuhiro I and Hirokazu K 2001 *Appl. Surf. Sci.* **169** 508
[27] Chopra K L, Major S and Pandya D K 1983 *Thin Solid Films* **102** 1
[28] Lu J G, Ye Z Z, Zeng Y J, Zhu L P, Wang L, Yuan J, Zhao B H and Liang Q L 2006 *J. Appl. Phys.* **100** 073714
[29] Choi B H, Im H B, Song J S and Yoon K H 1990 *Thin Solid Films* **193/194** 712
[30] Vanheusden K, Warren W L, Seager C H, Tallant D R, Voigt J A and Gnade B E 1996 *J. Appl. Phys.* **79** 7983
[31] Burstein E 1954 *Phys. Rev.* **93** 632
[32] Wang D, Liu Y C, Mu R, Zhang J Y, Lu Y M, Shen D Z and Fan X W 2004 *J. Phys.: Condens. Matter* **16** 4635
[33] Zhang Y, Lin B, Sun X and Fu Z 2005 *Appl. Phys. Lett.* **86** 131910
[34] Itoh T, Nishijima M, Ekimov A I, Gourdon C, Efros Al L and Rosen M 1995 *Phys. Rev. Lett.* **74** 1645